The potential use of the linear depolarization ratio to distinguish between convective and stratiform rainfall to improve radar rain-rate estimates

The Potential Use of the Linear Depolarization Ratio to Distinguish between Convective and Stratiform Rainfall to Improve Radar Rain-Rate Estimates

CAROLINE SANDFORD

Met Office, Exeter, United Kingdom

ANTHONY ILLINGWORTH AND ROBERT THOMPSON

University of Reading, Reading, United Kingdom

(Manuscript received 6 February 2017, in final form 3 August 2017)

ABSTRACT

A major source of errors in radar-derived quantitative precipitation estimates is the inhomogeneous nature of the vertical reflectivity profile (VPR). Operational radars generally scan in azimuth at constant elevation (PPI mode) and provide limited VPR information, so predetermined VPR shapes with limited degrees of freedom are needed to correct for the VPR in real time. Typical stratiform VPRs have a sharp peak below the 0° isotherm, known as the ''bright band,'' caused by the presence of large melting snowflakes, but this feature is not present in convective cores where the melting ice is in the form of graupel or compact ice. Inappropriate correction assuming a brightband VPR can lead to underestimation of rain rates, with particular impacts in intense convective storms. This paper proposes the use of high values of linear depolarization ratio (LDR) measurements to confirm the presence of large melting snowflakes and lower values for melting graupel or high-density ice as a prerequisite to selecting a suitable profile shape for VPR correction. Using a climatologically representative dataset of short-range, high-resolution C-band vertical profiles, the peak value of the LDR in the melting layer is shown to have robust skill in identifying VPRs without bright band, with the ''best'' performance at a threshold of −20 dB. Further work is proposed to apply this result to improving corrections for VPR at longer range, where the limited effect of beam broadening on LDR peaks could provide advantages over other available methods.

1. Introduction

Radar quantitative precipitation estimation (QPE) is achieved through the conversion of reflectivity measurements aloft into a rain-rate estimate at the ground. An important step in this process is determination and correction for inhomogeneities in the vertical profile of reflectivity (VPR).

The VPR defines the variation of atmospheric reflectivity with height above the ground surface. While there is little variation at low levels, other than that caused by partial beam blocking or orographic growth, in areas where the radar beam samples above or close to the 0° isotherm the difference between measured and surface reflectivities can exceed an order of magnitude. VPR is therefore a significant (if not the most significant) source of error in radar QPEs.

The vertical structure of precipitating systems varies with rain type. In stratiform conditions the VPR has a characteristic structure that includes the radar bright band: a region of enhanced reflectivity below the freezing level attributable to large melting snowflakes. However, there is a significant minority of cases in which no bright band exists: for example, in the presence of convection with graupel. Operational radars scan in plan position indicator (PPI) mode to provide good areal coverage, but because of horizontal variations in rain rate, it is very difficult to infer the VPR from PPI reflectivity values alone. Applying a brightband correction to radar data where none is present can lead to severely underestimated QPEs in hydrologically significant cases. Correctly identifying the underlying VPR type is therefore an important prerequisite for accurate correction and QPE.

The U.K. C-band radar network is currently being upgraded, with three-quarters of the network (as of December 2016) now delivering operational dual-polarization measurements. This increasing availability

Corresponding author: Caroline Sandford, caroline.sandford@metoffice.gov.uk

DOI: 10.1175/JAMC-D-17-0014.1

of high-quality dual-polarization data provides opportunities to improve the identification and correction for different types of VPR.

Existing VPR correction methods can generally be divided into ''global'' and ''local'' schemes. For global corrections the VPR shape is determined using data from large regions of the radar domain, sometimes over extended periods of time (e.g., Andrieu and Creutin 1995; Matrosov et al. 2007; Tabary 2007; Zhang and Qi 2010). This same VPR shape is then applied over extended domains and time periods. Local VPR schemes, by contrast, assume consistency over smaller regions, by azimuth sector, or rain-typed domain [e.g., Vignal et al. (1999), who define a local VPR scheme over 20 km × 20 km regions]. The more local the scheme is, the more closely it reflects true atmospheric conditions, with more local schemes tending to produce more accurate rainfall estimates (Vignal et al. 2000).

The Met Office radar processing software (Radarnet) uses a pixel-by-pixel VPR correction scheme developed by Kitchen et al. (1994). The mean stratiform profile shape (Fig. 1) was derived from a 3-yr climatological sample of high-resolution range–height indicator (RHI) scans observed with the 25-m S-band dish at Chilbolton, in southern England. The profile has a fixed brightband depth (of 700 m) and uses the wet-bulb freezing level from the Met Office's Unified Model with a grid length of 1.5 km (UKV; Brown et al. 2012) to define the top of the bright band. Mittermaier and Illingworth (2003) compared the forecast freezing-level height with observations of the melting-layer top from a vertically pointing radar, and found an RMS error of less than 150 m, confirming that the model height is sufficiently accurate for use in VPR correction. A single variable parameter in reflectivity is used to scale the idealized profile to the measured reflectivity at each radar pixel, using a known beam power profile to simulate the observed reflectivity measurement (Kitchen et al. 1994; Kitchen 1997) and adjusting the variable scaling parameter until the simulated reflectivity matches the observation. The surface reflectivity can then be found from the fitted profile.

A significant strength of the Met Office scheme is its ability to account for sub-kilometer-scale variability such as changes in brightband intensity and the presence of embedded convection, as it responds to local conditions at the radar radial resolution (600 m for the standard U.K. QPE) along each azimuth. Kitchen et al. (1994) demonstrated a 60% overall reduction in QPE error for a number of light stratiform cases, and emphasized that greater gains would be expected in heavier frontal rain. A similar improvement was found by Matrosov et al. (2007), who reported a 65% reduction in QPE in stratiform rainfall using a brightband correction

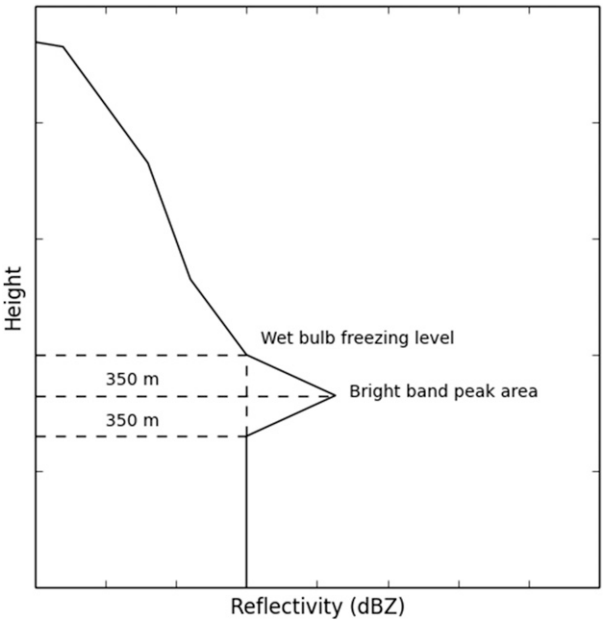

FIG. 1. The idealized stratiform VPR shape, derived by Kitchen et al. (1994), which is used operationally in Radarnet. The wet-bulb freezing level is derived from the operational forecast model gridded output.

scheme where the height of the melting layer was derived from the height of the minimum in the copolar correlation coefficient ρ_{hv}, rather than the height of the wet-bulb freezing level in the forecast model. However, the form of such idealized profiles is not suited to cases without bright band, such as occurs for example in embedded convection with graupel. The underestimation in surface rainfall caused by erroneous brightband correction disproportionately affects estimates of the intense, often flood-producing rainfall associated with convective cores. It is therefore important to identify where these profiles occur, to avoid errors in high-impact situations.

The current U.K. VPR scheme uses a high-level reflectivity threshold to identify profiles without bright band in radar data. If a reflectivity exceeding 30 dBZ is measured at a height exceeding 1 km above the wet-bulb freezing level (criterion hereinafter referred to as Z_1), the pixel is classified as convective, and the VPR at that pixel is set to be constant with height. This draws on the assumption that high reflectivities above the 0° isotherm can proxy for the strong updrafts associated with convection and non-brightband VPRs (Smyth and Illingworth 1998).

The majority of the VPR classification literature divides profiles into two broad types: stratiform (with bright band) and convective. Various schemes have been proposed to distinguish between these types in radar PPIs. The well-established method of Steiner et al. (1995)

uses the "intensity" and "peakedness" of the 2D radar reflectivity field as criteria to locate convective cores in 3-km constant-altitude PPIs (CAPPIs). These cores are then extended using a seeded growth algorithm, with any remaining rainfall classed as stratiform. This classification framework has formed the basis of much subsequent literature (e.g., Biggerstaff and Listemaa 2000; Anagnostou 2004; Rigo and Llasat 2004; Delrieu et al. 2009). Anagnostou (2004) presented a neural network scheme, adding parameters such as a vertical reflectivity gradient to the thresholds and texture parameters of Steiner et al. (1995), while Qi et al. (2013) developed a decision-tree approach using multisource data.

While reflectivity properties can be a useful indicator of precipitation type, they are indirect proxies, based on empirical studies of convective cells and bright bands. The scheme proposed by Steiner et al. (1995), for example, sets a minimum intensity of 40 dBZ to locate the center of a convective cell, yet a follow-up study by Delrieu et al. (2009) finds 43 dBZ to be more suitable. Both schemes are equally valid, since there is no direct physical link between the threshold reflectivity value and the presence of convection.

The justification of Steiner et al. (1995) in using horizontal reflectivity structure as a framework for convective diagnosis is based on the difficulty of detecting stratiform bright bands directly at long range. The authors identify smoothing of the reflectivity peak with range as the main limitation of a brightband approach, emphasizing also that strong reflectivity bright bands are often not measurable until the stratiform system is well developed. With the advent of dual-polarization measurements, however, measurements of reflectivity degraded by beam broadening are no longer the only available option.

One approach to convective diagnosis using dual polarization is to classify precipitation indirectly according to drop size distribution (DSD). Bringi et al. (2009) show that moments of a gamma DSD derived from reflectivity and differential reflectivity (ZDR) are distinctly different for stratiform and convective rain. Penide et al. (2013) find that this approach improves upon the Steiner et al. (1995) reflectivity-based classification algorithm. However, this and other DSD methods can only be applied to rain pixels and cannot classify measurements in and above the freezing level. In such cases the radar beam is already sampling rain, so no correction for VPR or bright band is required.

Recent papers have shown that the copolar correlation coefficient ρ_{hv} can be used to locate the melting layer in stratiform rainfall (e.g., Tabary et al. 2006; Matrosov et al. 2007; Giangrande et al. 2008; Boodoo et al. 2010). The increased variability of hydrometeor sizes, shapes, and orientations within the radar pulse volume due to melting is associated with a significant reduction in ρ_{hv}. However, the melting hail and graupel characteristics of convective melting layers also cause a similar reduction in ρ_{hv}. There are no published results to suggest that ρ_{hv} would be significantly different in stratiform bright bands from convective melting layers, where no bright band is present.

Smyth and Illingworth (1998) first suggested using the linear depolarization ratio (LDR) to distinguish between stratiform bright band and the deeper, mixed melting of higher-density graupel characteristic of convection. They classify stratiform events as having an LDR exceeding −18 dB (at S band) over widespread regions, corresponding to the bright band as sampled by radar PPIs. This high measured LDR occurs as a result of the strong depolarization properties of large melting snowflakes, which are also responsible for the stratiform reflectivity bright band. A major strength of LDR in brightband detection is that, since an LDR measurement is strongly dominated by the maximum depolarized reflectivity return, long-range LDR peaks are much less smoothed out by beam broadening (e.g., Fig. 2).

Since the dominant species of melting hydrometeors in convection is quasi-spherical graupel, which is much less depolarizing than melting snow, LDR has the potential to distinguish reliably between stratiform and convective melting. Illingworth and Thompson (2011) demonstrate the difference in peak melting-layer LDR for selected stratiform and convective case studies, and suggest that this finding could be extendable to a larger dataset. If so, using a direct, in situ LDR measurement to detect the different types of hydrometeor present in stratiform and convective melting has obvious benefits over a reflectivity-based proxy criterion.

The values of LDR can be affected by the differential attenuation of the returned horizontal- and vertical-polarization (H and V, respectively) signals. As for many operational radar systems, the Met Office uses the value of differential phase shift ϕ_{dp} to correct for two-way total attenuation. The two-way differential attenuation is about one-third of the total attenuation, but if necessary, the one-way differential attenuation could also be derived from ϕ_{dp} and used to correct for LDR.

This paper seeks to determine whether observations of LDR could potentially be used to distinguish cases of melting snow in stratiform bright bands from convective situations when there is no bright band. If this can be established, along with a suitable threshold value of LDR, then a different VPR correction scheme should be used for these two types of cases, as suggested by Illingworth and Thompson (2011).

The aim of this paper is to quantify the skill of using the maximum value of LDR in the melting layer to identify whether or not a bright band is present, in cases

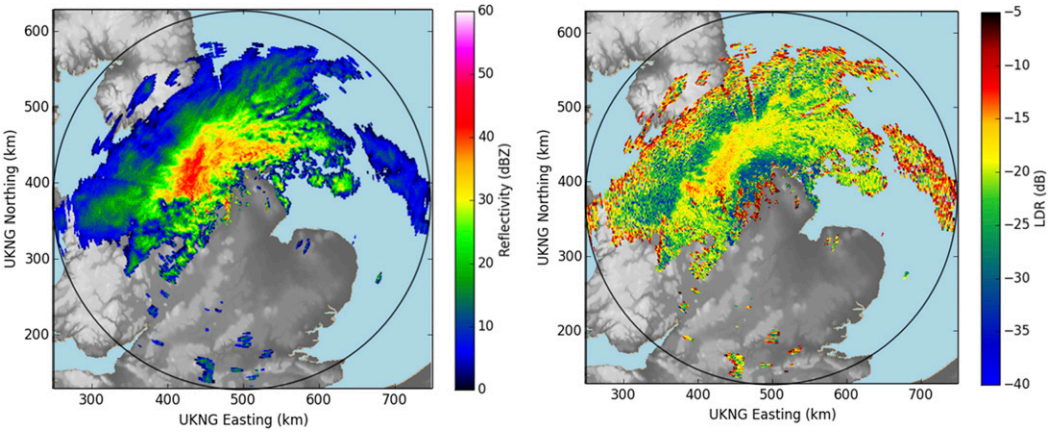

FIG. 2. Example (left) reflectivity and (right) LDR 0.5°-elevation PPIs from Ingham, 1709 UTC 21 Nov 2016, with a maximum range of 250 km. The clear bright band in LDR allows high reflectivity values around the radar to be correctly attributed either to a bright band (e.g., northwest of the radar) or to heavy rainfall (e.g., north and slightly east of the radar, at close range). The high values of LDR at long range are due to low signal-to-noise ratio.

where measurements are not affected by beam broadening. This is a prerequisite to further work on an algorithm to select the more suitable of ''stratiform'' (Fig. 1) or ''convective'' VPR shapes for correction at longer range. To address this question, a large sample of vertical profiles of reflectivity and LDR was extracted from RHI scans from the Met Office's C-band research radar at Wardon Hill. The profiles used are from short range only (5–15 km), to preserve the fine vertical structure and avoid any impacts of beam broadening. From these data, relative operating characteristic (ROC) curves are developed for both peak LDR and the current U.K. operational convective diagnosis criterion (Z_1), to compare skill and determine optimal LDR classification thresholds. Section 2 describes the dataset and methods used to extract a climatologically representative sample of vertical profiles. Section 3 presents results and discusses their implications. Section 4 concludes with a summary and outline of further planned work.

2. Dataset

To assess the skill of LDR in distinguishing between profile types, a large dataset of high-resolution vertical profiles was collected. For operational reasons, the radar scans primarily in PPI mode, so the data in this paper are obtained from an RHI performed every 10 min, when the radar moves down from the zenith after obtaining a ZDR calibration. Data over the range 5–15 km were used to obtain high-resolution vertical profiles unaffected by beam broadening, using the methods described in section 2a. Each vertical profile was assigned a ''true'' classification based on the reflectivity behavior in the melting region, to provide a baseline for assessing the skill of peak LDR.

a. *Extracting vertical profiles*

Upgraded radars within the Met Office network are capable of scanning in two dual-polarization modes. ''ZDR mode'' refers to simultaneous transmissions in the H and V channels, and is used for QPE. Additional ''LDR mode'' scans transmit in the horizontal polarization only, but receive in both the H and V channels. For low-elevation PPIs scanned at $8^\circ\,s^{-1}$, corresponding to 22 independent pulses per azimuth and range gate (after range averaging), the intrinsic limit on the accuracy of reflectivity is approximately 1.1 dB (Doviak and Zrnić 1993, p. 128), which (by summing in quadrature) yields an uncertainty on LDR of 1.5 dB.

The research radar at Wardon Hill performs an RHI scan in LDR mode every 10 min. An archive of these RHI scans was built up over two study periods: from late September to November 2014 and from April to August 2015. Absolute calibration of reflectivity was achieved to an accuracy of 1.5 dB by using the redundancy of Z, ZDR, and KDP in rain [self-consistency relation based on Gourley et al. (2009)]. LDR was calibrated to an accuracy of 0.5 dB or less by comparing the long-range noise emissions from sun interference, which is completely depolarized, in the H and V channels. The dataset was then filtered to remove both ''dry'' RHIs and those containing undesirable wide-ranging effects, such as radio frequency interference.

RHI data were collected by scanning through 0°–90° in elevation at a fixed azimuth, with a radial resolution of either 300 or 75 m. The scan duration was 17 s, with an average slewing rate of $5.3^\circ\,s^{-1}$. Azimuths were sampled

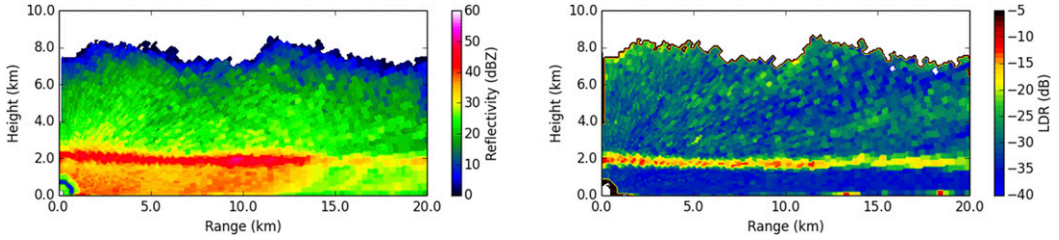

FIG. 3. Example stratiform RHI: (left) reflectivity and (right) LDR from 1416 UTC 13 Oct 2014, truncated at 10-km height and 20-km range. The bright band is clearly visible as a region of enhanced reflectivity and LDR at 2-km altitude, just below the 0°C isotherm (see also Fig. 6, top). Note that the bright band is clearly visible in LDR even at 15–20-km range, contrasting with the weaker reflectivity bright band in this region.

at random over the study period. The data in each scan consisted of the horizontally polarized reflectivity return Z, LDR, and clutter phase alignment (CPA) (Hubbert et al. 2009). CPA is a measure of the amplitude and phase variability of samples in the radar pulse volume and is significantly higher for stationary clutter than precipitation echoes.

To extract meteorological VPRs, a simple quality control procedure was developed to filter out nonmeteorological echoes. A pixel fulfilling the following criteria was classed as meteorological:

1) reflectivity $Z > 10\,\mathrm{dB}Z$,
2) LDR < -5 dB, and
3) CPA < 0.525.

All other pixels were discarded. The cross-polar isolation at the Wardon Hill radar, determined using the median LDR measurement in light rain (20–25 dBZ), is -36 dB. Given a noise threshold of $-20\,\mathrm{dB}Z$ at 15-km range, the reflectivity threshold of $10\,\mathrm{dB}Z$ corresponds to a minimum signal-to-noise ratio (SNR) of 30 dB; so the impact of cross-polar noise is negligible. Extending this sensitivity to a noise threshold $-3\,\mathrm{dB}Z$ at 100-km range, the SNR in the copolar channel for a reflectivity of $23\,\mathrm{dB}Z$ (equivalent to a rain rate of about 1 mm h^{-1}) would be 26 dB; so an LDR of -23 dB can be detected at 100 km. For more significant rain rates of 3 mm h^{-1} (about 31 dBZ), this LDR sensitivity would be achieved out to a range of 250 km.

Following quality control, the polar RHI data were regridded onto a Cartesian grid with 100 m $\times$ 100 m resolution. A very fine Cartesian grid was chosen so that the initial regridding could be done using a simple "nearest neighbor" algorithm. From this intermediate Cartesian grid, the data were then averaged to 1-km resolution in the horizontal. Vertical profiles were then extracted directly from the resulting 1 km (horizontal) $\times$ 100 m (vertical) grid. To preserve fine vertical structure and to minimize the effect of nonzero elevation on LDR, the profiles for this study were taken only from ranges between 5 and 15 km from the radar location. This resulted in a dataset of 6680 high-resolution vertical profiles, from 2283 RHIs taken on 104 different days.

b. Observed profile types

The vertical profile dataset was initially sorted into classes based on the shape of the reflectivity peak in the vicinity of the melting layer. For the purposes of this study only, since no ρ_{hv} data were available, a simple LDR-based algorithm was defined to locate the boundaries of melting in RHI profiles. By experimentation, the melting layer was defined as the region

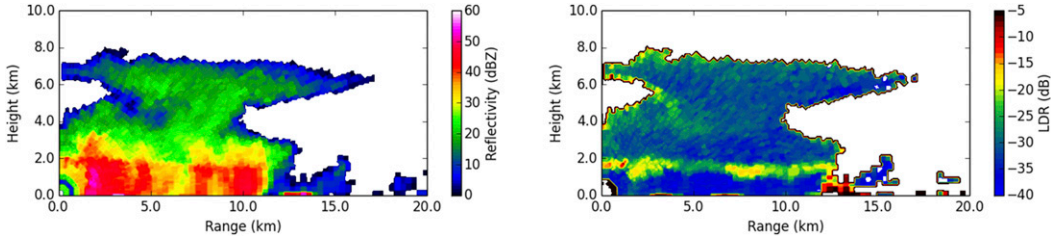

FIG. 4. Example RHI for rain from compact ice: (left) reflectivity and (right) LDR from 1346 UTC 9 Oct 2014, truncated at 10-km height and 20-km range. The compact-ice region around 5–7-km range shows no clear bright band in reflectivity, and correspondingly lower LDR than in the surrounding brightband regions. However, there is a sharp increase in reflectivity in the melting layer at 2-km altitude (see also Fig. 6, middle), which is not consistent with convective updrafts.

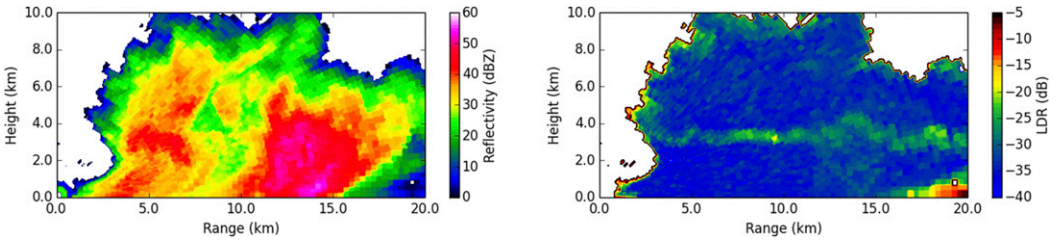

FIG. 5. Example convective RHI: (left) reflectivity and (right) LDR from 2220 UTC 3 Jul 2015, truncated at 10-km height and 20-km range. A weak bright band in the region of 8–10-km range, marking the 0°C isotherm at 3.5-km altitude (see also Fig. 6, bottom), contrasts sharply with the convection at 10–15 km. High reflectivity in this region extends consistently around 2 km above the melting layer. LDR values in the convective region are lower than in the weak brightband region and are much lower than in the strong brightband case in Fig. 3.

around the LDR peak where the LDR values and gradients met certain conditions. The process was as follows:

1) find the maximum measured LDR above the expected clutter height (300 m);
2) search downward from the peak for the melting layer base, where $\nabla\mathrm{LDR} < 20\,\mathrm{dB\,km^{-1}}$ and $\mathrm{LDR} < -25\,\mathrm{dB}$; the reflectivity at this point is Z_{rain}, and
3) search upward from the peak for the melting layer top, where $\nabla\mathrm{LDR} > -20\,\mathrm{dB\,km^{-1}}$ and $\mathrm{LDR} < -25\,\mathrm{dB}$; the reflectivity at this point is Z_{ice}.

The maximum reflectivity in the melting layer (between the heights of Z_{rain} and Z_{ice}) is then Z_{peak}, which is not usually collocated with the peak in LDR. The LDR gradient at a point was calculated over a 200-m-height window, between the values immediately above and below that point. The clutter height, LDR, and gradient thresholds were empirically determined using a selection of measured VPRs. This method was used only to automate the processing of this particular dataset, and there is no intention to extend it to any other context, given that robust threshold-based melting layer detection algorithms already exist for PPIs (e.g., Matrosov et al. 2007).

Initial analysis of a selection of RHIs and profiles suggested classification based on three categories. These categories align well with three of the five categories identified by Fabry and Zawadzki (1995) through an observational study using vertically pointing X-band radar:

1) *low-level rain*—shallow, light rainfall developing below the melting layer in stratiform conditions;
2) *rain with bright band*—cold rain developing above the 0° isotherm in stratiform conditions; this profile shows a clear increase in reflectivity with the onset of melting and decreasing Z below the melting layer, forming the traditional reflectivity bright band;
3) *rain from compact ice*—similar to the "rain with bright band" profile, in that increased reflectivity occurs with the onset of melting, but no decrease in Z is observed below the melting layer; Fabry and Zawadzki (1995) speculate that this profile shape "is likely caused by the melting of fast-falling snow pellets or dense graupels"; this is supported by later DSD analyses of Matrosov et al. (2016);
4) *showers*—shallow, light rainfall developing below the 0° isotherm in convective conditions; and
5) *deep convection*—the unstratified profiles observed where updrafts are present in convective thunderstorms, squall lines, and embedded convective cells.

The VPR dataset was sorted into three of these classes: rain with bright band (hereinafter "stratiform"; e.g., Fig. 3), compact ice (e.g., Fig. 4), and convective (e.g., Fig. 5). Both low-level rain and shower profiles, where the top of the precipitation profile was below the model freezing level (Brown et al. 2012), were excluded by design, since they do not include a melting layer.

The so-called true precipitation class for each VPR was determined based on the shape of the melting-layer peak. Figure 6 shows how the maximum reflectivity in the melting region (Z_{peak}) and at the top (Z_{ice}) and base (Z_{rain}) of the LDR-determined melting layer were compared. Classification rules were applied as follows:

1) if the peak-to-rain reflectivity difference $\Delta Z = Z_{\mathrm{peak}} - Z_{\mathrm{rain}} \geq 3$ dB, the profile is stratiform;
2) if $\Delta Z < 3$ dB and the peak-to-ice reflectivity difference $Z_{\mathrm{peak}} - Z_{\mathrm{ice}} \geq 6$ dB, the profile is compact ice;
3) otherwise, the profile is convective.

The choices behind these ΔZ and peak-to-ice classification thresholds are discussed in section 2c.

As expected for a high-latitude climate, the most prevalent profile in the Wardon Hill dataset is the stratiform profile, accounting for 84% of the total sample. Compact-ice profiles account for a further 10%, with 6% of profiles classed as convective. Examples of individual RHIs and profiles of each type are shown in Figs. 3–6. The average shapes of these profiles, along with quantiles to illustrate spread, are shown in Fig. 7.

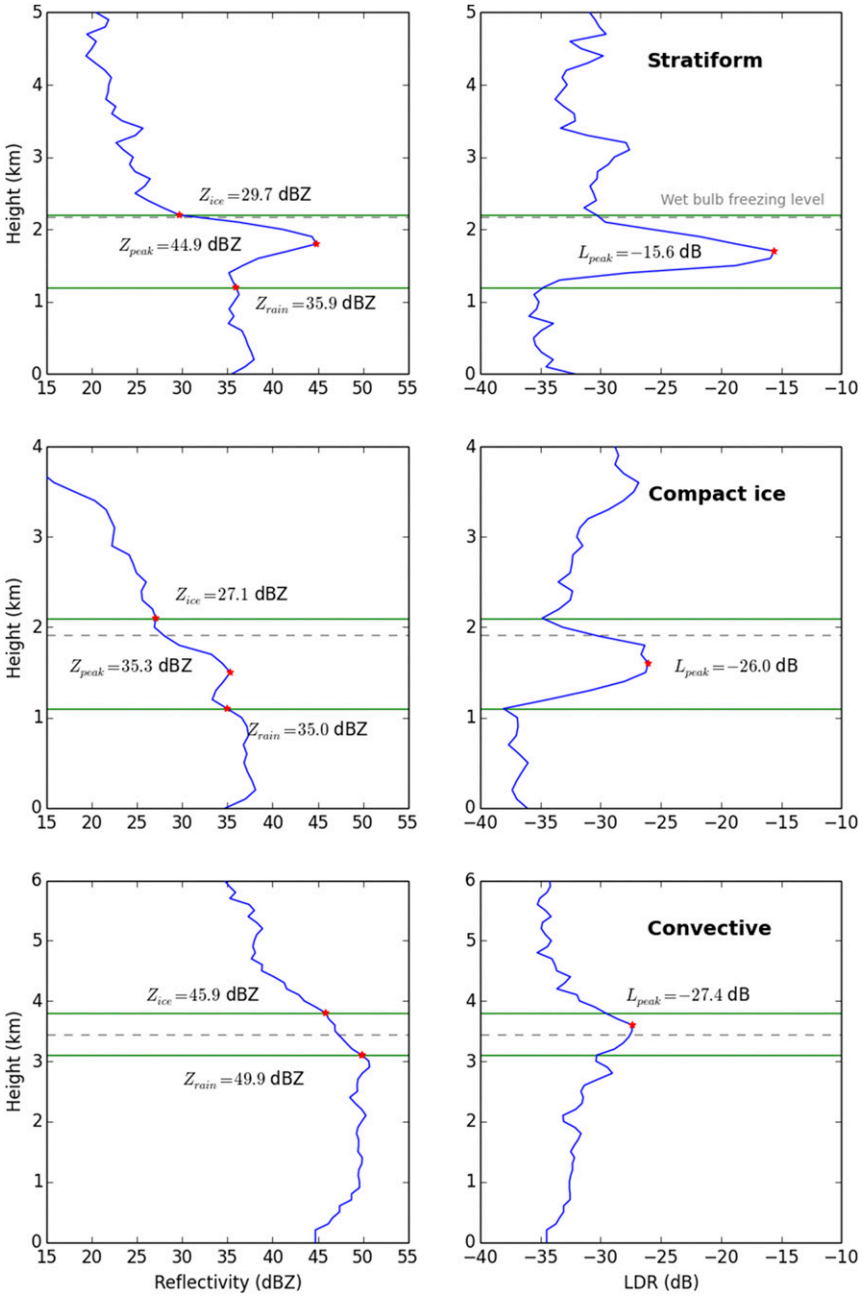

FIG. 6. (top) Vertical profiles of (left) reflectivity and (right) LDR from the stratiform RHI in Fig. 3 at 7.5-km range. (middle) As in the top panels, but from the compact-ice RHI in Fig. 4, at 5.5-km range. (bottom) As in the top panels, but from the convective RHI in Fig. 5, at 12.5-km range. Limits of the melting layer, as determined from the LDR profile, are shown in green, and the wet-bulb freezing level is represented by the dashed gray line. Annotated red stars show values at the key levels: reflectivity at the top (Z_{ice}) and bottom (Z_{rain}) of the melting layer, peaks (Z_{peak}) for stratiform and compact-ice cases, and the peak melting-layer LDR (L_{peak}).

Figure 8 shows the frequency distributions of rain reflectivity for the stratiform, compact-ice, and convective profiles used in this study. While small differences exist, the majority of these distributions occupy the same reflectivity region, with no significant difference in modal or mean values between the three profile types. This suggests that approaches based on reflectivity intensity may not be reliable in distinguishing between different types of VPR.

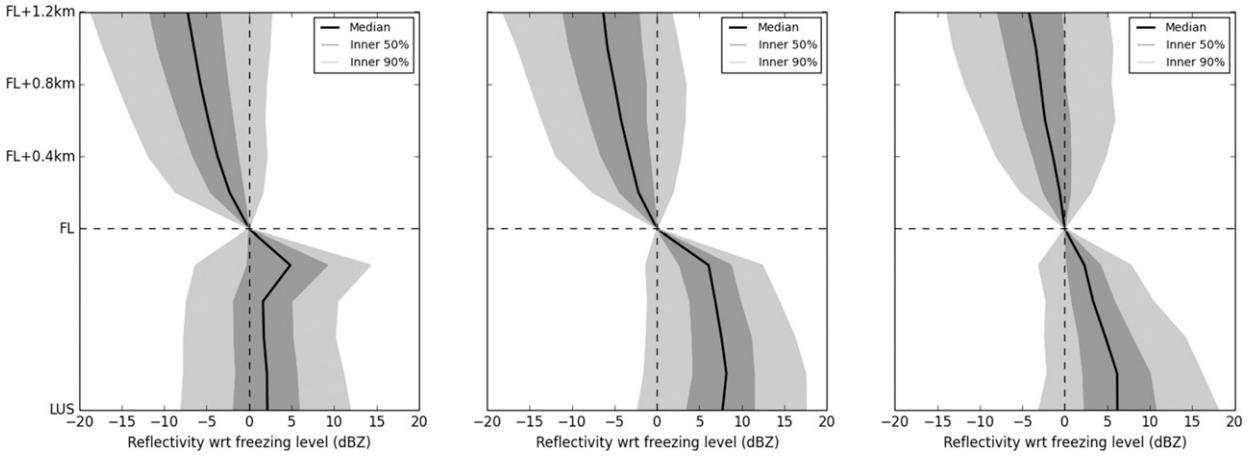

FIG. 7. Average stratiform, compact-ice, and convective reflectivity profiles with height relative to the model-derived (Brown et al. 2012) wet-bulb freezing level. Height levels are at six evenly spaced intervals between the lowest usable reflectivity (LUS) and the freezing level (FL), and then in 200-m steps above the FL.

c. *Quantitative definition of true VPR types*

The reflectivity peak size used to classify stratiform rain is based on observations of the profile sample, which showed some noise at the dBZ level. To account for this when determining the reflectivity peak, ΔZ exceeding 3 dB (a factor of 2 in linear reflectivity) was judged suitable for a profile to be classed as stratiform (with bright band).

The separation of compact-ice profiles from strong convection was more systematic. The physical explanation given by Fabry and Zawadzki (1995) for rain from compact ice involves dense, fast-falling ice and snow particles above the melting layer. These particles do not grow significantly as they melt, nor do they speed up, so the drop in reflectivity after melting observed in stratiform conditions does not occur. Recent observations of drop-size distributions by Matrosov et al. (2016) provide additional evidence in support of this model. The authors show that rain from compact ice (which they call "non bright band," as distinct from "bright band" and "convective" cases), has a much higher proportion of small drops than either stratiform or convective rain. This characteristic rain DSD would be consistent with a population of relatively small, dense ice or snow pellets in the region directly above the melting layer.

Using the standard assumption of no aggregation or breakup across the melting layer (e.g., Szyrmer and Zawadzki 1999; Hardaker et al. 1995), changes in reflectivity with melting can be attributed directly to changes in hydrometeor diameter, fall speed, and dielectric constant. The small, high-density ice particles responsible for compact-ice profiles are similar in both diameter and fall speed to liquid water, so the increase in reflectivity is almost entirely due to the increase in the dielectric factor. The squared ratio of the dielectric factors of ice and water then suggests a reflectivity increase of 7.2 dB with melting, or 6.5 dB if the slight difference in density between solid ice and water is taken into account. A minimum peak-to-ice threshold of 6 dB was therefore chosen to identify compact-ice profiles.

The use of approximate thresholds has the potential to impact the results of this study. If the reflectivity peak size thresholds are not well matched to the underlying

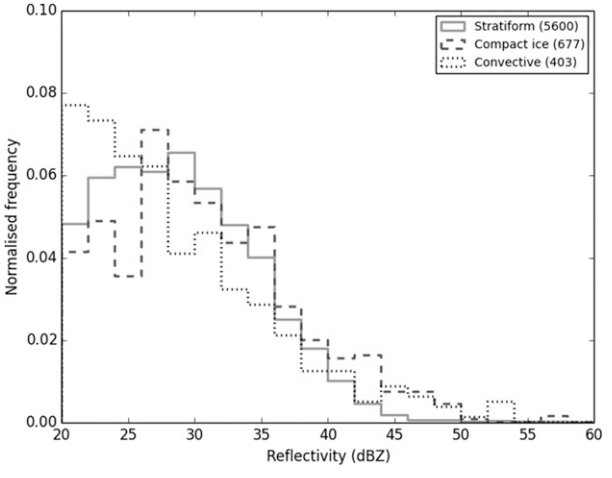

FIG. 8. Rain reflectivity frequency distributions for the stratiform, compact-ice, and convective VPRs used in this study. (The numbers in parentheses give the total number of each type of profile.) There is significant overlap between these distributions, with little difference in the mean or modal values. This suggests reflectivity-based criteria may not be effective in distinguishing between different types of VPR.

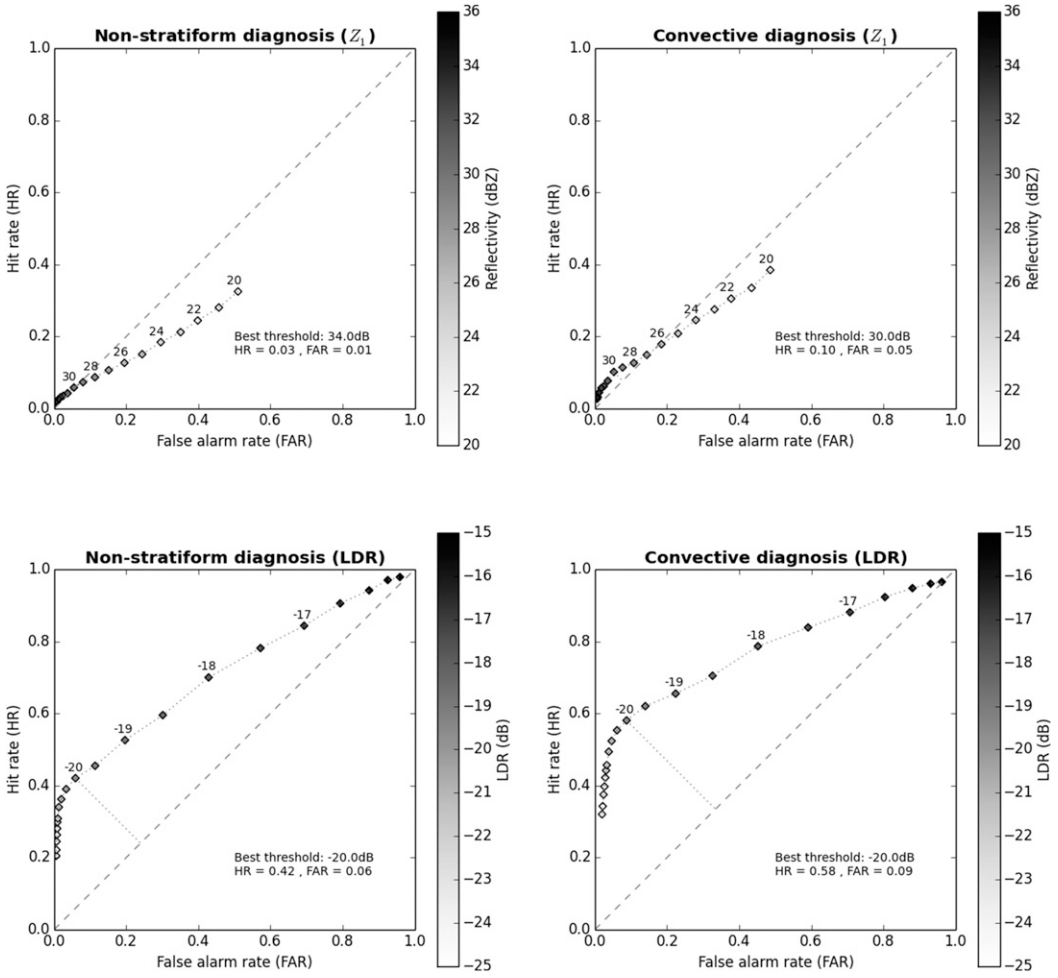

FIG. 9. ROC curves for (top) Z_1 thresholds from 20 to 36 dBZ and (bottom) peak LDR from −25 to −15 dB. (left) Skill in identifying nonstratiform profiles (compact ice and convective). (right) Skill in identifying convective profiles only. Plot points are gray-shade coded by the threshold used to classify profiles as nonstratiform (left panels) or convective (right panels), and some points have also been labeled by threshold.

physics, any discriminatory skill that LDR is found to have could be spurious, and the confidence in the best LDR peak threshold for profile identification would be low. To increase the robustness of the study results, a range of peak size thresholds will be tested around the selected values. These results are discussed alongside the main outcomes in section 3.

3. Results and discussion

The sample of profiles from 5–15-km range was classified by reflectivity peak as described in section 2b. A peak LDR value above any ground clutter, which can be uniquely attributed to melting, was then extracted for each profile and compared with the true classification (section 2b).

The intrinsic skill of LDR as a criterion was examined by comparing ROC curves for LDR with curves for the high-level reflectivity criterion Z_1. ROC curves above the 1:1 line demonstrate that a quantity has discriminatory skill, and the point farthest above the 1:1 line is the threshold at which that quantity most skillfully distinguishes between profile types. Contingency tables were generated for a range of LDR thresholds between −25 and −15 dB at 0.5-dB intervals, and for Z_1 from 20 to 36 dBZ at 1-dB intervals. Two sets of tables were generated: one for the diagnosis of all nonstratiform profiles (convection and compact ice) and the other for identifying convection only. Correct diagnosis of no bright band (or convection) is termed a hit, false identification of no bright band (or convection) is a false alarm, incorrect default to bright band is a miss, and correct default to a brightband profile is considered no detection. ROC curves, of hit rate (HR) against false-alarm rate (FAR), were then plotted for both types of categorization, with

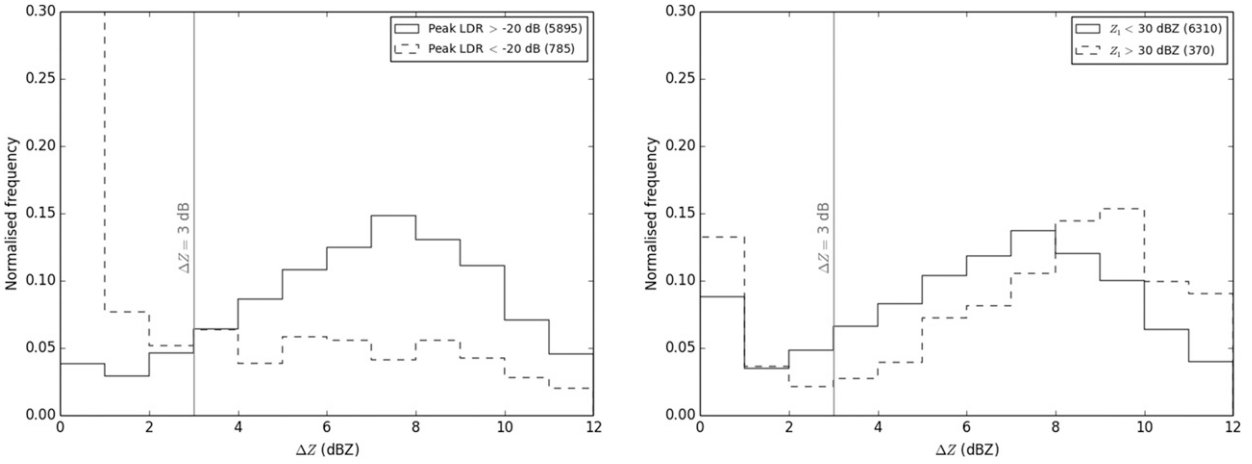

FIG. 10. Normalized frequency histograms of peak-to-rain (ΔZ) value for VPRs classified as bright band or non–bright band by (left) LDR and (right) Z_1. Dashed lines correspond to a non-brightband classification; solid lines correspond to stratiform VPRs. The figure in parentheses in each legend is the total number of profiles included in each histogram.

each point on the curve corresponding to a different threshold. HR and FAR are defined as follows:

$$\mathrm{HR} = \frac{\mathrm{Hits}}{\mathrm{Hits} + \mathrm{Misses}} \quad \text{and} \tag{1}$$

$$\mathrm{FAR} = \frac{\mathrm{False\ alarms}}{\mathrm{False\ alarms} + \mathrm{No\ detection}}. \tag{2}$$

ROC curves for the range of thresholds in peak LDR and Z_1 are shown in Fig. 9. The left-hand panel in Fig. 9 shows the skill of each criterion in identifying nonstratiform profiles, while the right-hand panel shows skill for convection only. The best threshold for identifying nonstratiform profiles, using a peak LDR of less than −20 dB, has an HR of 0.42 and a FAR of 0.06. By contrast, the currently operational high-level reflectivity criterion has virtually no skill in identifying nonstratiform profiles. A threshold of 34 dBZ gives a hit rate of 0.03, which was the highest above the corresponding rate of false alarms (0.01). The currently operational threshold of 30 dBZ has a higher hit rate (0.06), but this is equal to the rate of false alarms (0.06). The LDR criterion therefore gives a sevenfold increase in hit rate from the currently operational criterion, for no increase in FAR.

The distinguishing feature of stratiform profiles is the peak-to-rain ΔZ value that defines a bright band. The frequency distribution of ΔZ for profiles diagnosed as having no bright band should be peaked at very low values, while profiles with bright band will peak at higher positive values. Figure 10 shows normalized histograms of ΔZ in the high-resolution profile sample for stratiform and nonstratiform profile types, as diagnosed by LDR and Z_1, respectively. The ΔZ threshold for true profile classification of 3 dB is shown for reference. The LDR histograms are well separated, with the distribution of brightband ΔZ peaked at 7–8 dB, and non-brightband profiles heavily skewed toward $\Delta Z < 1$ dB. However, the Z_1 histograms are much less well separated. The brightband histogram is similar to that obtained from LDR; however, the profiles diagnosed as non–bright band by Z_1 show a bimodal distribution in ΔZ, with equally high normalized frequencies in both $\Delta Z < 1$ dB and the 8–10-dB window. This further demonstrates the lack of intrinsic skill in Z_1, and the improvements achievable by using LDR.

The right-hand panels in Fig. 9 show the respective skill of LDR and Z_1 in separating convection from other types of VPR (stratiform bright band and compact ice). Convective VPRs are skillfully identified by a peak LDR of −20 dB, with an HR of 0.58 and a FAR of 0.09. By comparison, Z_1 shows minimal skill; the best threshold for convection (of 30 dBZ) has an HR of 0.10 and a FAR of 0.05.

High reflectivity kilometers above the freezing level is considered to be a proxy for strong updrafts and large rimed hydrometeor species, such as hail. The lack of skill of Z_1 in identifying compact-ice profiles is consistent with the expected microphysics, since compact-ice profiles arise from a different DSDs than other types of profile (Fabry and Zawadzki 1995; Matrosov et al. 2016), and not from convective processes. However, the lack of skill in identifying convective profiles is unexpected and suggests that reflectivity at this height is, in fact, a poor proxy for updrafts and riming.

Sensitivity to VPR-type definitions

Section 2c presents the peak size thresholds used to define reflectivity profiles as stratiform, compact ice, or convective. These thresholds of 3 and 6 dB for ΔZ and

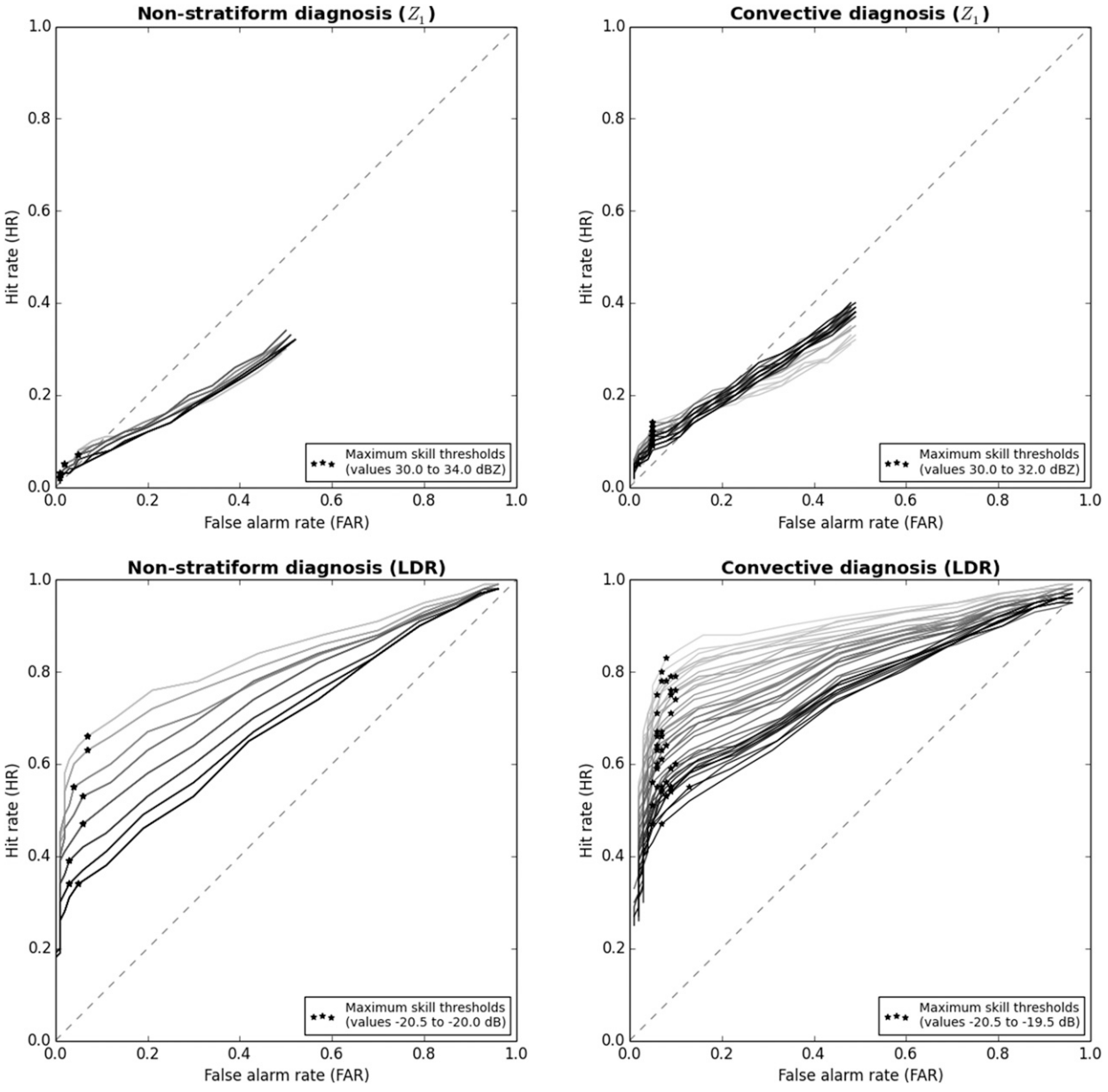

FIG. 11. As in Fig. 9, but for the ROC curves for (top) Z_1 thresholds from 20 to 36 dBZ and (bottom) peak LDR from −25 to −15 dB, for the range of true-classification ΔZ and peak-to-ice values tested in the sensitivity study. Lighter gray shades correspond to smaller ΔZ and peak-to-ice thresholds (see also Fig. 12).

peak-to-ice reflectivity differences, respectively, were subjectively determined and, therefore, have some inherent uncertainty. The ''best'' LDR threshold of −20 dB, and the qualitative skill of LDR as a parameter (as measured by an ROC curve consistently above the 1:1 line), should not be sensitive to small changes in VPR peak size thresholds within this uncertainty range. Consistency in the best LDR value for profile discrimination would increase confidence in the finding that LDR has skill and in the inference that this skill is derived through a response to a physical process: that is, the melting of large snowflakes.

To test the sensitivity of LDR skill to the precise definition of VPR types, additional ROC curves were generated for a range of peak size thresholds. The minimum ΔZ needed to define a profile as stratiform was varied between 0.5 and 4.0 dB (eight test values), and peak-to-ice thresholds ranged from 4.0 to 8.0 dB (five test values).

Figures 11 and 12 show the range of ROC curves generated from the 40 different sets of thresholds used

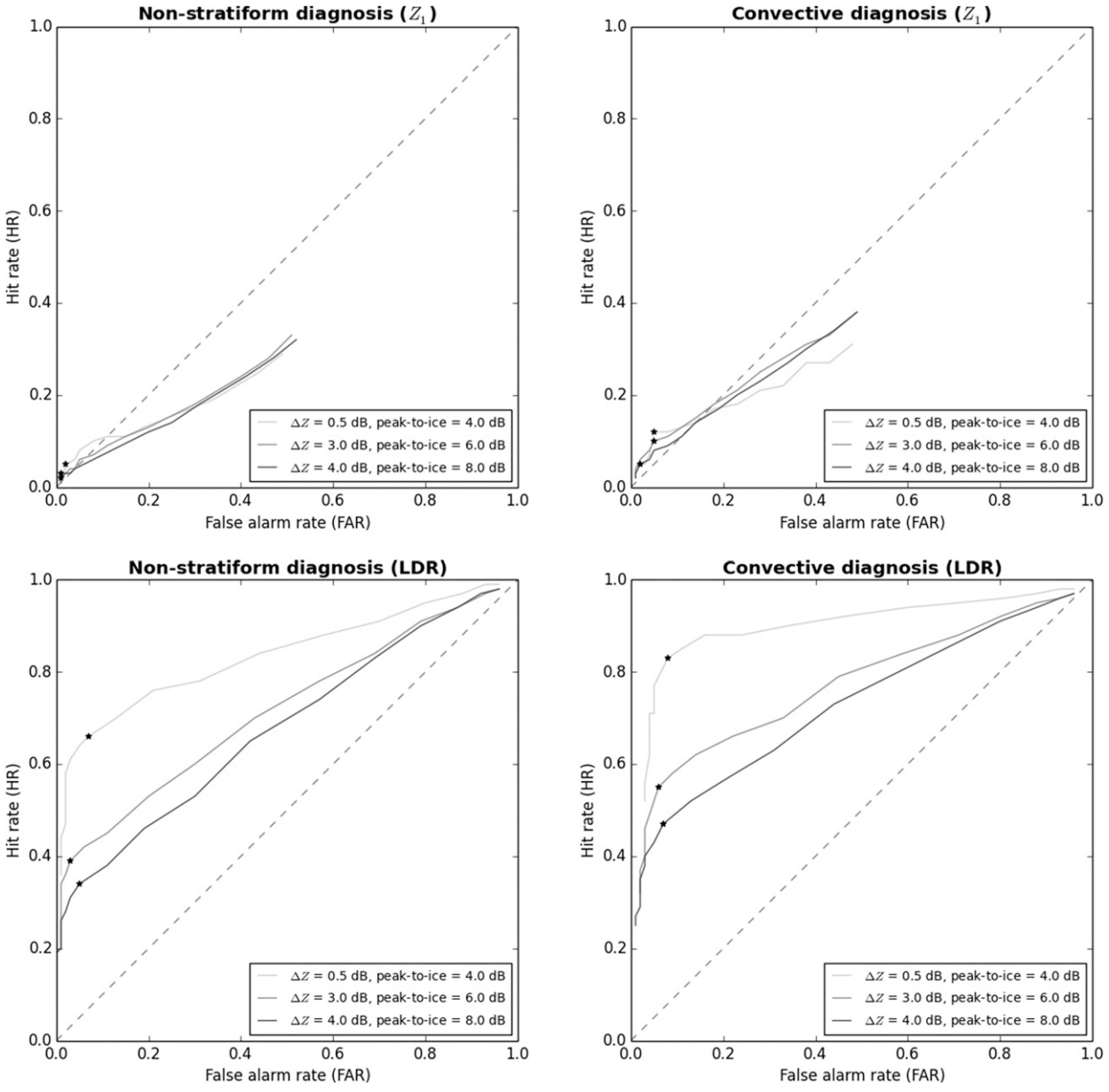

FIG. 12. As in Figs. 9 and 11, but for ROC curves for (top) Z_1 thresholds from 20 to 36 dBZ and (bottom) peak LDR from −25 to −15 dB, for extremes of the sensitivity study shown fully in Fig. 11. Curves are labeled by threshold values to illustrate trends. (Note that the gray scale here does not match Fig. 11.)

in the sensitivity study. (For the identification of no-brightband profiles, only 8 of the 40 curves are visible in Fig. 11. This is because the no-brightband identification is not sensitive to the peak-to-ice threshold, so the five peak-to-ice curves for each ΔZ threshold are identical.) It can be seen that, although the positions of the curves differ, all LDR threshold curves are consistently above the 1:1 line. The maximum skill threshold for identifying nonstratiform and convective profiles in LDR is robust to uncertainty in true profile definitions, having a value of -20 ± 0.5 dB for all combinations of tested thresholds. By contrast, there is no combination of thresholds for which Z_1 shows skill in distinguishing between profile types.

From these data it can be concluded that LDR skill is not sensitive to the precise dividing lines between VPR types as defined by the size of the reflectivity peaks but is a robust indicator of the presence of large melting snowflakes leading to stratiform bright bands.

4. Conclusions

Accurate determination and correction for VPR in operational radar data requires a priori information as to the profile shape, which varies with precipitation type. Before VPR correction, precipitation measurements are often separated into convective or stratiform types, using different shapes to determine and correct for the VPR in different conditions. Current algorithms developed to diagnose convection, such as the well-established Steiner et al. (1995) reflectivity-based method, use proxies for convective updrafts and cores, and may not be reliably transferrable between radar systems or climatologies.

This paper assesses the potential benefits of LDR measurements in distinguishing between different types of VPR. LDR responds directly to the presence of the large melting snowflakes responsible for the reflectivity bright band. Values of LDR in the melting layer vary with precipitation type, showing lower values in nonstratiform regions where melting species originate from higher-density ice.

In this work a large sample of high-resolution vertical reflectivity and LDR profiles was collected and classified into three types, corresponding to three of the types identified by Fabry and Zawadzki (1995). This dataset of 6680 profiles was used to assess the skill of peak melting-layer LDR in distinguishing between VPRs with and without bright bands.

It has been demonstrated that peak LDR has skill over a range of values, significantly greater than the skill of the high-level reflectivity threshold currently used in the United Kingdom. A peak LDR value of −20 dB was found to maximize the probability of detection of nonstratiform profiles for a given FAR. This result suggests LDR has the potential to effect large improvements in the operational identification of nonstratiform reflectivity profiles. This will reduce the underestimation of rain rates because of inappropriate brightband correction, with particular benefits expected through preserving the high precipitation intensities associated with convective cores.

Having established the ability of LDR to distinguish between stratiform and non-brightband melting, the authors will pursue research toward an operational implementation for the Met Office radar processing software. Examining long-range values of LDR in PPI mode is expected to confirm the negligible effect of beam broadening on peak values (Smyth and Illingworth 1998), so the detection of brightband melting at long ranges should be significantly improved where LDR—in addition to reflectivity—is available. One way to do this would be to compare the simultaneous values of LDR in PPIs observed at two different elevations from overlapping radars, so that the bright band is much closer to one radar than the other. Where possible, comparing LDR PPIs with RHIs in stratiform conditions could provide further verification of the accuracy of long-range LDR measurements. By exploiting LDR measurements to select suitable VPR shapes, the authors expect to improve operational correction for VPR in nonstratiform conditions, increasing the accuracy of the corresponding surface QPEs. Within the context of operational QPEs, it would be useful in the future to explore the potential of ρ_{hv} for this application.

Acknowledgments. This project was partially funded by the European Regional Development Fund through INTERREG IVb, as part of the RAINGAIN project. The authors also thank Dawn Harrison for helpful advice and feedback.

REFERENCES

Anagnostou, E., 2004: A convective/stratiform precipitation classification algorithm for volume scanning weather radar observations. *Meteor. Appl.*, **11**, 291–300, doi:10.1017/S1350482704001409.

Andrieu, H., and J. D. Creutin, 1995: Identification of vertical profiles of radar reflectivity for hydrological applications using an inverse method. Part I: Formulation. *J. Appl. Meteor.*, **34**, 225–239, doi:10.1175/1520-0450(1995)034<0225:IOVPOR>2.0.CO;2.

Biggerstaff, M., and S. Listemaa, 2000: An improved scheme for convective/stratiform echo classification using radar reflectivity. *J. Appl. Meteor.*, **39**, 2129–2150, doi:10.1175/1520-0450(2001)040<2129:AISFCS>2.0.CO;2.

Boodoo, S., D. Hudak, N. Donaldson, and M. Leduc, 2010: Application of dual-polarization radar melting-layer detection algorithm. *J. Appl. Meteor. Climatol.*, **49**, 1779–1793, doi:10.1175/2010JAMC2421.1.

Bringi, V., C. Williams, M. Thurai, and P. May, 2009: Using dual-polarized radar and dual-frequency profiler for DSD characterization: A case study from Darwin, Australia. *J. Atmos. Oceanic Technol.*, **26**, 2107–2122, doi:10.1175/2009JTECHA1258.1.

Brown, A., S. Milton, M. Cullen, B. Golding, J. Mitchell, and A. Shelly, 2012: Unified modeling and prediction of weather and climate: A 25-year journey. *Bull. Amer. Meteor. Soc.*, **93**, 1865–1877, doi:10.1175/BAMS-D-12-00018.1.

Delrieu, G., B. Boudevillain, J. Nicol, B. Chapon, and P. Kirstetter, 2009: Bollene-2002 experiment: Radar quantitative precipitation estimation in the Cevennes–Vivarais region, France. *J. Appl. Meteor. Climatol.*, **48**, 1422–1447, doi:10.1175/2008JAMC1987.1.

Doviak, R., and D. Zrnić, 1993: *Doppler Radar and Weather Observations.* 2nd ed. Academic Press, 562 pp.

Fabry, F., and I. Zawadzki, 1995: Long-term radar observations of the melting layer of precipitation and their interpretation. *J. Atmos. Sci.*, **52**, 838–851, doi:10.1175/1520-0469(1995)052<0838:LTROOT>2.0.CO;2.

Giangrande, S., M. Krause, and A. Ryzhkov, 2008: Automatic designation of the melting layer with a polarimetric prototype of the WSR-88D radar. *J. Appl. Meteor. Climatol.*, **47**, 1354–1364, doi:10.1175/2007JAMC1634.1.

Gourley, J., A. Illingworth, and P. Tabary, 2009: Absolute calibration of radar reflectivity using redundancy of the polarization observations and implied constraints on drop shapes. *J. Atmos. Oceanic Technol.*, **26**, 689–703, doi:10.1175/2008JTECHA1152.1.

Hardaker, P., A. Holt, and C. Collier, 1995: A melting-layer model and its use in correcting for the bright band in single-polarization radar echoes. *Quart. J. Roy. Meteor. Soc.*, **121**, 495–525, doi:10.1002/qj.49712152303.

Hubbert, J., M. Dixon, S. Ellis, and G. Meymaris, 2009: Weather radar ground clutter. Part I: Identification, modeling, and simulation. *J. Atmos. Oceanic Technol.*, **26**, 1165–1180, doi:10.1175/2009JTECHA1159.1.

Illingworth, A., and R. Thompson, 2011: Radar bright band correction using the linear depolarisation ratio. *Eighth Int. Symp. on Weather Radar and Hydrology*, Exeter, United Kingdom, International Association of Hydrological Sciences, 64–68, http://www.met.reading.ac.uk/radar/publications/LDR.pdf.

Kitchen, M., 1997: Towards improved radar estimates of surface precipitation rate at long range. *Quart. J. Roy. Meteor. Soc.*, **123**, 145–163, doi:10.1002/qj.49712353706.

——, R. Brown, and A. Davies, 1994: Real-time correction of weather radar data for the effects of bright band, range and orographic growth in widespread precipitation. *Quart. J. Roy. Meteor. Soc.*, **120**, 1231–1254, doi:10.1002/qj.49712051906.

Matrosov, S., K. Clark, and D. Kingsmill, 2007: A polarimetric radar approach to identify rain, melting-layer, and snow regions for applying corrections to vertical profiles of reflectivity. *J. Appl. Meteor. Climatol.*, **46**, 154–166, doi:10.1175/JAM2508.1.

——, R. Cifelli, P. Neiman, and A. White, 2016: Radar rain-rate estimators and their variability due to rainfall type: An assessment based on hydrometeorology testbed data from the southeastern United States. *J. Appl. Meteor. Climatol.*, **55**, 1345–1358, doi:10.1175/JAMC-D-15-0284.1.

Mittermaier, M. P., and A. J. Illingworth, 2003: Comparison of model-derived and radar-observed freezing-level heights: Implications for vertical reflectivity profile-correction schemes. *Quart. J. Roy. Meteor. Soc.*, **129**, 83–95, doi:10.1256/qj.02.19.

Penide, G., A. Protat, V. Kumar, and P. May, 2013: Comparison of two convective/stratiform precipitation classification techniques: Radar reflectivity texture versus drop size distribution-based approach. *J. Atmos. Oceanic Technol.*, **30**, 2788–2797, doi:10.1175/JTECH-D-13-00019.1.

Qi, Y., J. Zhang, and P. Zhang, 2013: A real-time automated convective and stratiform precipitation segregation algorithm in native radar coordinates. *Quart. J. Roy. Meteor. Soc.*, **139**, 2233–2240, doi:10.1002/qj.2095.

Rigo, T., and M. Llasat, 2004: A methodology for the classification of convective structures using meteorological radar: Application to heavy rainfall events on the Mediterranean coast of the Iberian Peninsula. *Nat. Hazards Earth Syst. Sci.*, **4**, 59–68, doi:10.5194/nhess-4-59-2004.

Smyth, T. J., and A. J. Illingworth, 1998: Radar estimates of rainfall rates at the ground in bright band and non-bright band events. *Quart. J. Roy. Meteor. Soc.*, **124**, 2417–2434, doi:10.1002/qj.49712455112.

Steiner, M., R. Houze Jr., and S. Yuter, 1995: Climatological characterization of three-dimensional storm structure from operational radar and rain gauge data. *J. Appl. Meteor.*, **34**, 1978–2007, doi:10.1175/1520-0450(1995)034<1978:CCOTDS>2.0.CO;2.

Szyrmer, W., and I. Zawadzki, 1999: Modeling of the melting layer. Part I: Dynamics and microphysics. *J. Atmos. Sci.*, **56**, 3573–3592, doi:10.1175/1520-0469(1999)056<3573:MOTMLP>2.0.CO;2.

Tabary, P., 2007: The new French operational radar rainfall product. Part I: Methodology. *Wea. Forecasting*, **22**, 393–408, doi:10.1175/WAF1004.1.

——, A. Le Henaff, G. Vulpiani, J. Parent-du Chatelet, and J. J. Gourley, 2006: Melting layer characterisation and identification with a C-band dual-polarization radar: A long term analysis. *Fourth European Conf. on Radar in Meteorology and Hydrology*, Barcelona, Spain, Center of Applied Research in Hydrometeorology (CRAHI), http://www.crahi.upc.edu/ERAD2006/proceedingsMask/00005.pdf.

Vignal, B., H. Andrieu, and J. D. Creutin, 1999: Identification of vertical profiles of reflectivity from volume scan radar data. *J. Appl. Meteor.*, **38**, 1214–1228, doi:10.1175/1520-0450(1999)038<1214:IOVPOR>2.0.CO;2.

——, G. Galli, J. Joss, and U. Germann, 2000: Three methods to determine profiles of reflectivity from volumetric radar data to correct precipitation estimates. *J. Appl. Meteor.*, **39**, 1715–1726, doi:10.1175/1520-0450-39.10.1715.

Zhang, J., and Y. Qi, 2010: A real-time algorithm for the correction of brightband effects in radar-derived QPE. *J. Hydrometeor.*, **11**, 1157–1171, doi:10.1175/2010JHM1201.1.